An Experimental Testbed for the Study of Visual Based Navigation Docking of Two Vertical Compound Aircraft

DONG WANG [1,2], **QIZHEN HONG** [2,3], **JING WANG** [1], **HERAN SUN** [2,4],
LUCHAO CHENG [1,2], **MINGYANG LI** [1,2], **CONGJING WANG** [1,2],
XIN HUANG [1,2], **ZHIYUAN WANG** [1,2], **AND JIAHANG LI** [5]

[1] Changchun Institute of Optics, Fine Mechanics and Physics, Chinese Academy of Sciences, Key Laboratory of Space-based Dynamic and Rapid Optical
Imaging Technology, Chinese Academy of Sciences, Changchun 130033, China
[2] University of Chinese Academy of Sciences, Beijing 100049, China
[3] State Key Laboratory of High Temperature Gas Dynamics, Institute of Mechanics, Chinese Academy of Sciences, Beijing 100190, China
[4] Changchun Institute of Optics, Fine Mechanics and Physics, Chinese Academy of Sciences, Changchun 130033, China
[5] Teli College, Beijing Institute of Technology, Beijing 100081, China

Corresponding author: Jing Wang (wangjing@ciomp.ac.cn)

ABSTRACT Compound aircraft, merging the advantages of two or more aircraft, is now a promising concept for designing modern aircraft. How to achieve successful docking of two aircraft in flight is an important issue for the applications of vertical compound aircraft. In order to resolve such an issue, this paper proposes a new visual based navigation docking scheme, which is different from rendezvous and docking operations in space applications. The present scheme uses a monocular camera mounted on the chaser aircraft with a certain installation angle to collect the visual features of the target aircraft, then the position and attitude of the landing gear of the target aircraft can be determined. Moreover, a six degrees of freedom docking mechanism mounted on the chaser aircraft is designed to catch hold of the landing gear tires of the target aircraft. In order to avoid undesired collision during the docking process, Z-direction position of the target landing gear is predicted and the proposed Z-direction speed control algorithm is applied to the chaser platform. The robustness of the present scheme has been validated numerically and experimentally by means of a chaser platform and a target platform on the ground testbed. Successful docking of the chaser platform and the target landing gear has been achieved, respectively, when the target platform performs a Z-direction movement and a compound movement.

INDEX TERMS Compound aircraft, collision avoidance, docking process, visual based navigation.

I. INTRODUCTION

In order to possess the capabilities of long distance flight, vertical take-off and landing, etc., a new concept called Multi-functional Compound Aircraft (similar to Compound Aircraft Transport, CAT [1]) was proposed by combining two or more aircraft and using the resources of each other to achieve a specific flight goal. By doing this, the performance of the compound aircraft can be promoted through taking the unique advantage of each single aircraft and the design of each single aircraft can be greatly simplified.

Lots of works have been devoted to develop the compound aircraft, which can be roughly divided into two categories, i.e., horizontal compound aircraft and vertical compound aircraft. A horizontal compound scheme, by connecting two aircraft wingtip-to-wingtip, has been proposed and tested for several years [1], [2]. Reference [2] summarizes a couple of projects related to the horizontal compound aircraft. The wingtip-docked configuration increases the total span of the aircraft system and thus gains significant aerodynamic benefits [1].

Besides horizontal compound aircraft, the proposal of vertical compound aircraft has also been studied. A reusable horizontal take-off/horizontal landing two-stage-to-orbit vertical compound aircraft has been designed to reduce the

launch costs and bring payloads into low-earth orbit safely and economically [3], the feasibility of this concept is tested through a high-fidelity simulation. Besides above application, the concept of vertical compound of two aircraft (upper and lower aircraft) allows the upper aircraft to have the capability of vertical take-off and landing, as long as the lower aircraft provides enough lift force. Thus the upper aircraft can carry more fuel and fly a longer distance.

The challenge facing the vertical compound aircraft is to safely accomplish the docking process of upper and lower aircraft. Nevertheless, the study about the dynamic docking process of aircraft in flight is much fewer than the study concerning the space rendezvous and docking operations [4]–[6]. Ref. [7] reported the flight test of the docking of a Douglas C-47A cargo aircraft and a small Q-14B target plane, pilots manually operated the aircraft to complete the docking by the wingtip locking devices of the two aircraft. The above flight test of docking process is only concerned with horizontal compound aircraft, the research on docking process between vertical compound aircraft is still scarce in the literature.

Undesired collision must by all means be avoided during close proximity docking process of aircraft, thus a robust collision-free navigation scheme is needed. Among others, the automated visual based navigation scheme has been investigated widely and gradually become an indispensable tool to achieve the success of docking. Most applications of visual based techniques were well studied and tested for orbital rendezvous operations in Refs. [8]–[10], the authors prove the reliability and effectiveness of the technique. Recently a novel visual based approach combining with deep learning method was introduced in Ref. [11] to estimate the 6-DOF pose of uncooperative spacecraft in the application of proximity operations using monocular-vision measurement, the proposed approach achieved competitive pose estimation performance in real-time but does not be applied to actual docking process yet. In addition to above studies, the visual based techniques were also used in other scenarios. Ref. [12] reported a navigation control algorithm based on monocular-vision for the autonomous landing of a quadrotor on a moving mobile platform and Ref. [13] investigated a docking navigation method for autonomous aerial refueling of unmanned aerial vehicles based on a binocular vision system.

During the two aircraft docking process, external perturbation resulting from incoming air flow and wing-to-wing coupling [14] would cause low frequency oscillations in position and attitude of the aircraft. Despite the fact that modern aircraft has greatly improved the ability of handling and stability, aforementioned unsteady external perturbation and time delay of operation still make the human intervention unpractical, thus the automated navigation is needed. In view of many advantages (as mentioned above) of visual based technique, it becomes an excellent candidate for automated navigation [10], [15] and is also used in present work.

With the aim to achieve successful docking of two vertical compound aircraft, a new automated visual based navigation docking scheme is proposed in this paper. In present scheme,
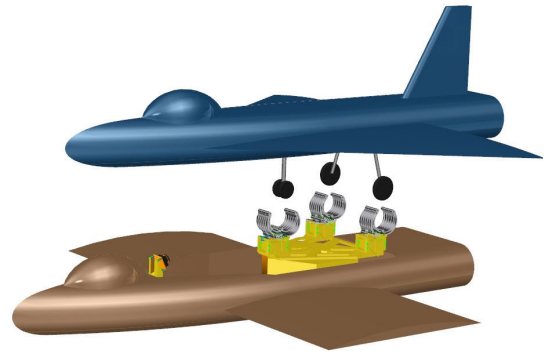

FIGURE 1. Schematic diagram of present visual based navigation scheme for the docking of two aircraft in flight (the upper aircraft is the target aircraft and the lower one is the chaser aircraft).

as shown in Fig. 1, a six degrees of freedom (6-DOF) docking mechanism mounted on the chaser aircraft (lower one) is designed to catch hold of landing gear tires of the target aircraft (upper one). When two aircraft approach each other (which is unsteady process with continuous variation of their relative position and attitude), monocular camera fixed at the chaser aircraft collects the visual features of landing gear tires of the target aircraft. Moreover, solving the position and attitude of the target landing gear tires based on monocular vision is considered as a perspective-three-point (P3P) problem, which can be effectively solved by the algebraic approach or the geometric approach [16]–[19]. During the chasing process, by analyzing position and attitude of the target landing gear tires at current time step, a new path planning algorithm proposed in this paper then drives the docking mechanism to chase predicted position of the target landing gear tires at next time step, in the meanwhile speed control algorithm is also applied to the docking mechanism.

The main contributions of this paper are as follows:

1. An experimental ground testbed, composed of a chaser platform and a target platform, was built for the study of the new proposed automated visual based navigation docking scheme. The soundness of present scheme has been proved both numerically and experimentally.

2. The present scheme meets the requirements of most vertical compound aircraft and has high versatility. Most of the aircraft install three target landing gears underneath the fuselage in the shape of isosceles triangle, the position and attitude of this kind of structural feature can be identified precisely using present scheme.

3. Path and attitude planning algorithm is proposed, which is the key to avoid undesired collision during the docking process.

The paper is organized as follows: Section II introduces experimental setup of the testbed; Section III gives details about theory and numerical simulation method of visual based navigation; Section IV describes speed control strategies during the chasing process of the chaser platform; Section V reports docking experiments when the target platform is performing a Z-direction movement and a compound
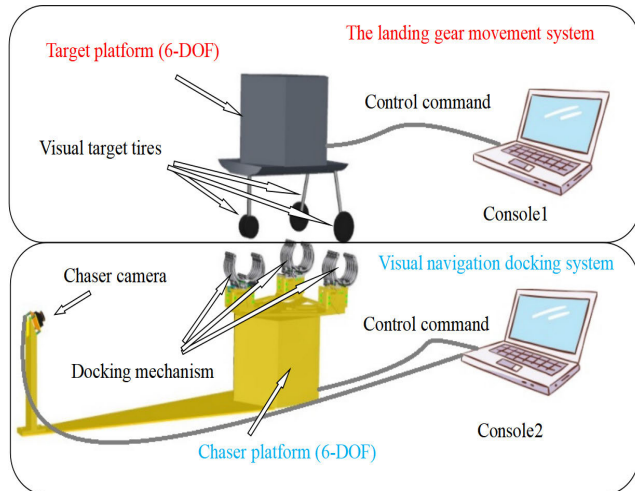
FIGURE 2. Schematic diagram of the ground experimental testbed with two consoles controlling the target landing gear movement system and the visual navigation docking system, respectively.

FIGURE 3. The visual navigation docking system of the chaser platform (lower) and the target platform (upper) which is suspended above the chaser platform.

FIGURE 4. Architecture diagram of the visual based navigation docking system.

movement, respectively; Concluding remarks are given in Section VI.

II. THE EXPERIMENTAL TESTBED

In order to reproduce the docking process of two aircraft, the experimental testbed is made of two main parts, as shown in Fig. 2, i.e., a movement system (called target platform, consisting of an upside-down 6-DOF platform with landing gear tires) and a visual based navigation docking system (called chaser platform, consisting of monocular camera and a 6-DOF platform with a docking mechanism). The upside-down 6-DOF platform (carrying landing gear tires) of the target platform simulates the complex three-dimensional (3-D) relative motion of two aircraft in flight, while a 6-DOF platform is also designed on the chaser platform to adjust position and attitude of the docking mechanism during the chasing process. Moreover, two consoles are used to analyze the collecting data of above two platforms separately and release control command.

A. THE TARGET PLATFORM

Figure 3 shows the actual target platform (upper one in the figure). When the landing gear is fully opened, its position with respect to the aircraft is generally no longer changed. Therefore in present experiment it is enough to only simulate the critical parts of the target aircraft, namely the landing gear moving with a 6-DOF platform, so that there is no need to make any modifications to the original structure of the target aircraft when the soundness of present scheme is proved. Moreover, the landing gear tire has a relatively simple shape (mostly showing rectangular or oval in the image, see also next Section), thus it is convenient for visual feature recognition. Furthermore, since the landing gear is a three-points supporting structure, the isosceles triangle formed by the midpoints of the tires is conducive to attitude algorithm.
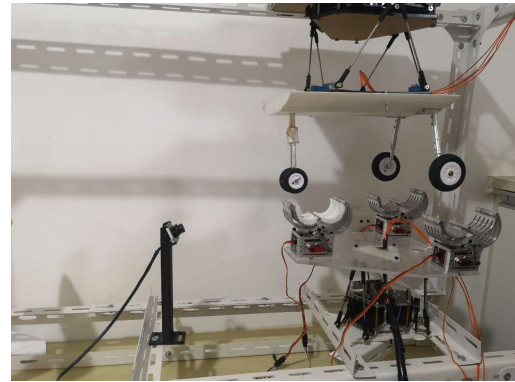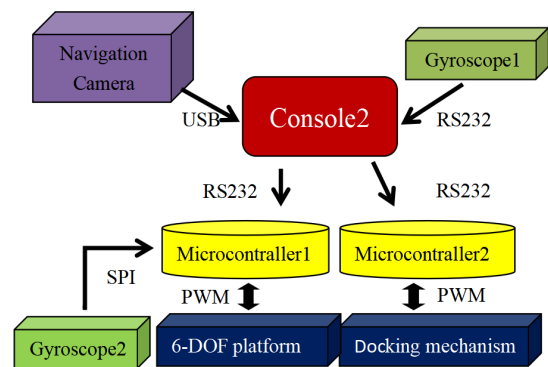
In present experiment the target platform is able to make 3-D movement to reproduce the condition when the aircraft is suffering from unexpected external perturbation. In general, the relative motion of two aircraft during the docking process is compound movement (low frequency) with changing the relative position and attitude continuously, thus the 6-DOF platform of the target platform can simulate the real situation as much as possible.

B. THE CHASER PLATFORM

The actual visual based navigation docking system (called chaser platform, see the lower one in Fig. 3), consisting of Console 2, 6-DOF platform, docking mechanism and navigation camera, is more complex than the above target platform. In present experiment the chaser platform is designed to simulate the chasing process and test the feasibility of proposed path planning algorithm and speed control strategy. The control logic architecture of the visual based navigation docking system is depicted in Fig. 4. Specifically, the Gyroscope 1 is used to detect attitude of the 6-DOF platform, then collected data are transmitted to Console 2. Monocular camera fixed at the front of the chaser platform with a certain installation angle is used to acquire image and recognize

visual target, then collected data are transmitted to the Console 2. After gathering all the data, Console 2 solves the position and attitude of the target platform, plans the chasing path of the chaser platform and controls the chasing speed. The command from Console 2 is thus transmitted to Microcontroller 1 (performing closed-loop control of the 6-DOF platform through the attitude feedback from the Gyroscope 2) and Microcontroller 2 (driving the docking mechanism to lock the landing gear tires).

The system dynamics of the chaser platform is mainly determined by the 6-DOF platform, whose dynamic model is discussed in detail in Ref. [20]. In present experiment, the Console 2 sends command to the chaser platform every 0.04 second (this time interval is related to the hardware performance such as the transmission Baud rate, 115200 symbol/s in this case). According to default maximum speed, 20 mm/s (see Section IV-B), of the chaser platform, it can be calculated that the maximum displacement is less than 1 mm within 0.04 second. Moreover, the measured overshoot of the 6-DOF platform when moving 1 mm is 9.6%, and the measured settling time is 0.014 second. Therefore the 6-DOF platform used in present experiment is stable and robust.

III. VISUAL BASED NAVIGATION

The visual based navigation docking process is achieved when the docking mechanism of the chaser platform successfully catches hold of three landing gear tires of the target platform. During this process, monocular camera acquires image and recognizes the visual features (see Fig. 5) of landing gear tires, then the relative configuration (namely position and attitude) between the target platform and the chaser platform can be determined by theoretical solution. In present experiment, the camera (staying static during the whole process since only the 6-DOF platform of the chaser platform is moving, which is a new approach different from the one used in space rendezvous operations [5]) is fixed on the chaser platform and kept a certain elevation angle (λ, see Fig. 6).
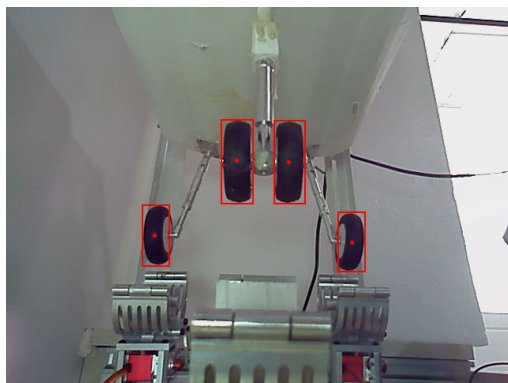

FIGURE 5. Schematic diagram of visual features of the landing gear tires.

In what follows, theories related to visual based navigation are introduced, i.e., theory of solving the position and attitude
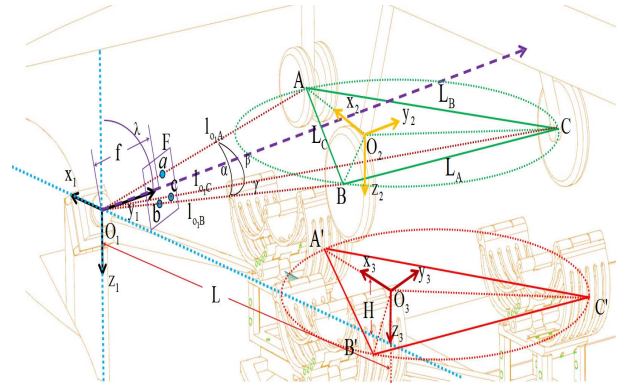

FIGURE 6. Reference frames used in present P3P problem.

of the target landing gear based on monocular vision and theory of solving the chasing path of the chaser platform.

A. THEORY
1) SOLVING POSITION AND ATTITUDE BASED ON MONOCULAR VISION

The distances between the landing gear tires are known by calibration. As shown in Fig. 5, the front landing gear has two tires but only the midpoint of them is adopted in the visual processing. Moreover, each single tire of the rear landing gear has an individual midpoint, thus solving the position of above three points can be considered as a P3P problem. The unique positive solution of the P3P problem can only be obtained under certain conditions [16]. According to these conditions one can then appropriately adjust the position and elevation angle of the monocular camera, so that the valid range of unique solution is broaden.

Three different reference frames are defined in present P3P problem (see Fig. 6 for clarity). The camera is the origin of the navigation docking coordinate system ($O_1 x_1 y_1 z_1$), the center of the circumcircle formed by three midpoints of the landing gear tires is the origin of the target coordinate system ($O_2 x_2 y_2 z_2$), and the center of the circumcircle formed by three points of the docking mechanism is the origin of the chaser coordinate system ($O_3 x_3 y_3 z_3$). The variables in Fig. 6 can be classified into different groups as follows:

- *known parameters (determined by design or calibration)*:
  - X_3, Y_3, Z_3: coordinate values of point O_3 in the coordinate system $O_1 x_1 y_1 z_1$;
  - L, H: X coordinate and Z coordinate values of point O_3 in the coordinate system $O_1 x_1 y_1 z_1$ at the initial state;
  - L_A, L_B, L_C: length of line segment BC, AC, AB;
  - F: image plane;
  - f: camera focal length;
  - λ: elevation angle of camera.
- *variables measured via image processing*:
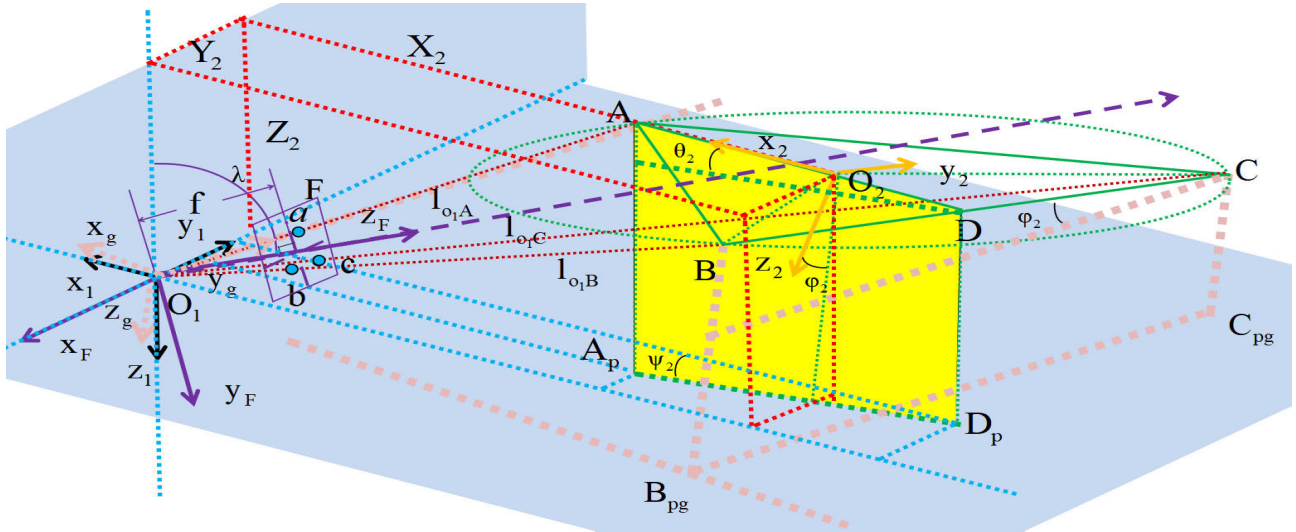 - F_a, F_b, F_c: the position of a, b, c on the image plane F.

FIGURE 7. Geometric diagram of position and attitude solution based on P3P problem.

- $l_{O_1a}, l_{O_1b}, l_{O_1c}, l_{ab}, l_{ac}, l_{bc}$: length of line segment $O_1a, O_1b, O_1c, ab, ac, bc$.

- *variables to be determined (see Fig. 7):*
  - X_2, Y_2, Z_2: coordinate values of point O_2 in the coordinate system $O_1x_1y_1z_1$;
  - $\varphi_2, \theta_2, \psi_2$: roll, pitch, and yaw angles of the coordinate system $O_2x_2y_2z_2$ in the coordinate system $O_1x_1y_1z_1$.

As seen in Fig. 7, the coordinate value of a point on the image plane F is (x_F, y_F, f) in the coordinate system $(O_1x_Fy_Fz_F)$, whose Z axis is perpendicular to the image plane. According to the scale of pixel size, one can get the coordinate values of three characteristic points (a, b, c on the plane F), i.e., $a(x_{aF}, y_{aF}, f)$, $b(x_{bF}, y_{bF}, f)$ and $c(x_{cF}, y_{cF}, f)$. Then the lengths of $l_{O_1a}, l_{O_1b}, l_{O_1c}, l_{ab}, l_{ac}, l_{bc}$ can be obtained using above coordinate values. Moreover, the cosine values of α, β and γ (indicated in Fig. 6) are simply computed as follows:

$$
\begin{cases}
\cos \alpha = \dfrac{l_{O_1a}^2 + l_{O_1b}^2 - l_{ab}^2}{2\, l_{O_1a} l_{O_1b}} \\[2mm]
\cos \beta = \dfrac{l_{O_1a}^2 + l_{O_1c}^2 - l_{ac}^2}{2\, l_{O_1a} l_{O_1c}} \\[2mm]
\cos \gamma = \dfrac{l_{O_1b}^2 + l_{O_1c}^2 - l_{bc}^2}{2\, l_{O_1b} l_{O_1c}}.
\end{cases}
\tag{1}
$$

Furthermore, the positive solution of $l_{O_1A}, l_{O_1B}, l_{O_1C}$ can be calculated [18]:

$$
\begin{cases}
l_{O_1B} = l_{O_1A} \cos \alpha + \sqrt{L_C^2 - l_{O_1A}^2 \sin \alpha} \\[2mm]
l_{O_1C} = l_{O_1A} \cos \beta + \sqrt{L_B^2 - l_{O_1A}^2 \sin \beta} \\[2mm]
l_{O_1B}^2 + l_{O_1C}^2 - 2\, l_{O_1B} l_{O_1C} \cos \gamma = L_A^2.
\end{cases}
\tag{2}
$$

Then by using the proportional relationship of the sides of similar triangles, one have

$$
\begin{cases}
A\,(x_{AF}, y_{AF}, z_{AF}) = a\,(x_{aF}, y_{aF}, z_{aF}) \times 1_{O_1A}/1_{O_1a} \\
B\,(x_{BF}, y_{BF}, z_{BF}) = b\,(x_{bF}, y_{bF}, z_{bF}) \times 1_{O_1B}/1_{O_1b} \\
C\,(x_{CF}, y_{CF}, z_{CF}) = c\,(x_{cF}, y_{cF}, z_{cF}) \times 1_{O_1C}/1_{O_1c}.
\end{cases}
\tag{3}
$$

Thus the coordinate values of points A, B and C in the coordinate system $O_1x_1y_1z_1$, i.e. $A(x_A, y_A, z_A)$, $B(x_B, y_B, z_B)$ and $C(x_C, y_C, z_C)$, can be determined by the transformation relationship between coordinate systems $O_1x_1y_1z_1$ and $O_1x_Fy_Fz_F$. Finally the coordinate values of point O_2 (X_2, Y_2, Z_2) in the coordinate system $O_1x_1y_1z_1$ can be determined when coordinates of A, B and C are known.

Furthermore, the roll, pitch and yaw angles $(\varphi_2, \theta_2, \psi_2)$ are obtained in the following way. Firstly, line segment AD (D is the midpoint of line segment BC) is introduced in Fig. 7, the coordinate value of point D (x_D, y_D, z_D) in the coordinate system $O_1x_1y_1z_1$ can be easily calculated via points B and C. Thus the pitch angle θ_2 can be simply obtained as $\theta_2 = \arctan\left[(z_A - z_D)/\sqrt{(x_A - x_D)^2 + (y_A - y_D)^2}\right]$.

In order to calculate the roll and yaw angles, points A and D are projected onto the plane $x_1O_1y_1$ and become points A_p and D_p, then it is seen that the yaw angle ψ_2 is the angle between the projection line A_pD_p and the axis O_1x_1, that is to say $\psi_2 = \arctan\left[(y_A - y_D)/(x_A - x_D)\right]$. In addition, the roll angle φ_2 is the angle between the plane AA_pD_pD and the axis O_2z_2, and can be obtained through following coordinate transformations. The new coordinate system $O_1x_gy_gz_g$ is defined by firstly rotating the coordinate system $O_1x_1y_1z_1$ through angle ψ_2 around the O_1z_1 axis and followed by rotating angle θ_2 around the O_1y_1 axis. Therefore the coordinate values of points B (x_{Bg}, y_{Bg}, z_{Bg}) and C (x_{Cg}, y_{Cg}, z_{Cg}) in the new coordinate system $O_1x_gy_gz_g$ can be determined, then the roll angle φ_2 is easily computed as $\varphi_2 = \arctan\left[(z_{Bg} - z_{Cg})/(y_{Bg} - y_{Cg})\right]$.

FIGURE 8. Schematic diagram of four representative phases of chaser platform during the chasing process.

2) THE ALGORITHM FOR SOLVING THE CHASING PATH

During the chasing process, the chaser platform needs to plan its chasing path in order to avoid blocking the sight of camera, otherwise it will result in the fact that the position and attitude of the target landing gear tires are not able to solve. Fig. 8 shows four representative phases of the chaser platform during the chasing process:

1) phase 1 to 2, the chaser platform is moving straight up without any adjustment of attitude;
2) phase 2 to 3, the chaser platform is adjusting its position and attitude by path planning in order to avoid blocking the sight of camera;
3) phase 3 to 4, the chaser platform is adjusting its position and attitude through analyzing the data at phase 3, and finally accomplishes the docking.

The variables in Fig. 8 can be classified into different groups as follows:

- *known parameters:*
  - L_{C1}: X_1 direction distance from point O_3 to point O_1;
  - L_{C0}: distance from the foremost point of the docking mechanism to point O_1 in the X_1 direction;
  - H_C: height of the docking mechanism;
  - a_c: distance from the foremost point of the docking mechanism to point O_3;
  - β_0: acute angle between the line a_c and the bottom plane of the docking mechanism;
  - L_{T1}: X_1 direction distance from point O_2 to point O_1;
  - R_{T1}: perpendicular distance between point O_2 and the line connecting the two rear landing gear tires;
  - H_T: Z_1 direction distance from point O_2 to point O_3 at phase 4;
  - h_{CT}: Z_1 direction distance from point O_2 to point O_3 at phase 1;
  - r: radius of the landing gear tire.

- *intermediate variables in calculation:*
  - β_1: acute angle of the line (connecting the midpoint of the rear landing gear tires to point O_1) with respect to the X_1 axis;
  - β_2: acute angle of the line (connecting the midpoint of the rear landing gear tires to point O_1) with respect to line segment r;
  - β_b: acute angle of the line (connecting center point of the chaser platform at phase 2 and the one at phase 3) with respect to the X_1 axis.

- *variables to be determined:*
  - h_C: distance moved from phase 1 to phase 2 in the Z_1 direction;
  - H_{CX}: distance moved from phase 2 to phase 3 in the X_1 direction;
  - H_{CZ}: distance moved from phase 2 to phase 3 in the Z_1 direction;
  - β_C: acute angle between the line (connecting the lowest visible point of the rear landing gear tire to point O_1) and the X_1 axis.

The first class of variables are the parameters solved by monocular vision or inherent parameters of the chaser platform and the target landing gear, which can be considered as known value in present calculation. The third class of variables can then be simply obtained by geometric relations (see Fig. 8):

$$\begin{cases} \beta_1 = \arctan\left(h_{CT}/\left(L_{T1}+R_{T1}\right)\right) \\ \beta_2 = \arccos\left(r/\left(h_{CT}/\sin\beta_1\right)\right) \\ \left(90° - \beta_c\right) + \left(\beta_1 + \beta_2\right) = 180° \\ h_C = L_{C0} \times \tan\beta_c \\ \beta_b = 180° - \beta_0 - \left(180° - \beta_c\right)/2 \\ H_{CX} = 2\,a_c \times \sin\left(\beta_c/2\right) \times \cos\beta_b \\ H_{CZ} = 2\,a_c \times \sin\left(\beta_c/2\right) \times \sin\beta_b. \end{cases} \quad (4)$$

Therefore it is possible to determine the amount of movement during the chasing process. To be more specific, the amount of movement from phase 1 to phase 2 (along the negative Z_1 direction) is h_C. From phase 2 to phase 3, the amount of movement along the negative X_1 direction is H_{CX}, along the negative Z_1 direction is H_{CZ} and the amount of clockwise rotation around the Y_1 axis is $\boldsymbol{\beta}_C$. From phase 3 to phase 4, the amount of movement along the positive X_1 direction is H_{CX}, along the negative Z_1 direction is $(H_C + h_{CT}) - (H_{CZ} + h_c + H_T)$ and the amount of counterclockwise rotation around the Y_1 axis is $\boldsymbol{\beta}_C$.

B. IMAGE PROCESSING

The main steps of image feature recognition are described in the following. First of all, the camera acquires the RGB image, which is then converted to gray image. Next, one should filter out areas with low grayscale value in the gray image by closed operation, and then binary the image. However, in some cases, there still exists some features unrelated to the actual tires in the binarized image. Thus an extra step is needed by using the edge extraction algorithm to extract edges in the binarized image, then the extracted edge is highlighted by gray lines in the image. Next step is to compare those edges obtained in the image with the edge feature of actual tire, consequently the correct tire edges are recognized by setting the threshold value. Finally, the midpoints of the selected feature edges are found. An example of present image processing procedure is shown in Fig. 9.
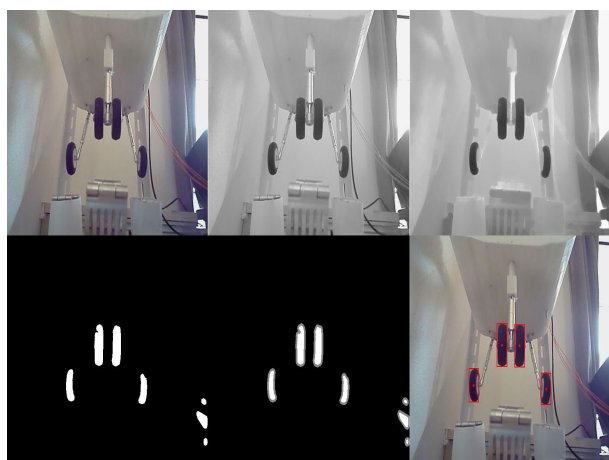
FIGURE 9. RGB image (upper left), gray image (upper middle), closed operation (upper right), binarized image (lower left), edge extraction (lower middle), tire feature recognition (lower right).

The present algorithm is tested by experiment. With the variation of position (X, Y, Z displacement) and attitude (rolling, pitching, yawing motion), respectively, the recognized tire features are shown in Fig. 10 and Fig. 11. The obtained tire features are used to compute position and attitude of the target landing gear tires according to the algorithm described in last subsection. Comparing the calculated

position and attitude with the reference ones shows good agreement between them, except that the error value of the roll angle is quite large (see the points of "Uncorrected error" in Fig. 12) in the yawing motion, which is due to the large offset of the recognized tire midpoint (see the lower panel of Fig. 11). Such a large error value (increasing with yaw angle) is unacceptable during the chasing process, thus a linear function (the dashed line in Fig. 12) is proposed in present algorithm to correct the roll angle, and it turns out that the sampling accuracy can be improved to within 0.5 (see the points of "Corrected error" in Fig. 12).

C. SIMULATED TEST FOR SOLVING POSITION AND ATTITUDE

The performance of the algorithm proposed in Section III-A1 is tested based on Matlab simulation. The position and attitude obtained by the algorithm is compared to the reference values, so that the valid range of obtaining unique positive solution of P3P problem is determined. It is seen from Fig. 13 that the position error (of X-axis displacement under the X-axis motion, of Y-axis displacement under the Y-axis motion and of Z-axis displacement under the Z-axis motion) between simulation results and reference results is near zero (within 0.02 mm since the actual errors coming from installation, noise, acquisition deviation cannot be reproduced in the simulation) and the case of multiple solutions does not occur. However, the attitude error (of roll angle under the rolling motion, of pitch angle under the pitching motion and of yaw angle under the yawing motion) between simulation results and reference results is only near zero (within 0.02) within a certain range. Specifically, the valid range for the unique solution of pitch angle is $[-70, 37]$, of roll angle is $[-89, 89]$ and of yaw angle is $[-48, 48]$. Generally the variation of attitude angles of the target aircraft is small and will not exceed the range of 15 in actual flight, thus the present algorithm to solve the position and attitude is valid in general cases.

D. EXPERIMENTAL TEST FOR SOLVING POSITION AND ATTITUDE

The performance of the algorithm proposed in Section III-A1 is tested experimentally on the experimental testbed. The experimental results (in the coordinate system $O_1 x_1 y_1 z_1$) are shown in Fig. 14, which is also compared with the reference value to get the error value (see Fig. 15). The number of sampling points is related to the maximum variation range of each component of the 6-DOF platform. It is seen from Fig. 15 that the error range of X-axis displacement is within 1.5mm under the X-axis movement, of Y-axis displacement is within $[-1.5mm, 0.5mm]$ under the Y-axis movement and of Z-axis displacement is within $[-1.5mm, 0mm]$ under the Z-axis movement. Moreover, the error range of roll angle is within $[0.15, 0.9]$ under the rolling motion, of pitch angle is within $[-0.3, 0.1]$ under the pitching motion and of yaw angle is within $[-0.15, 0.2]$ under the yawing motion. It should be
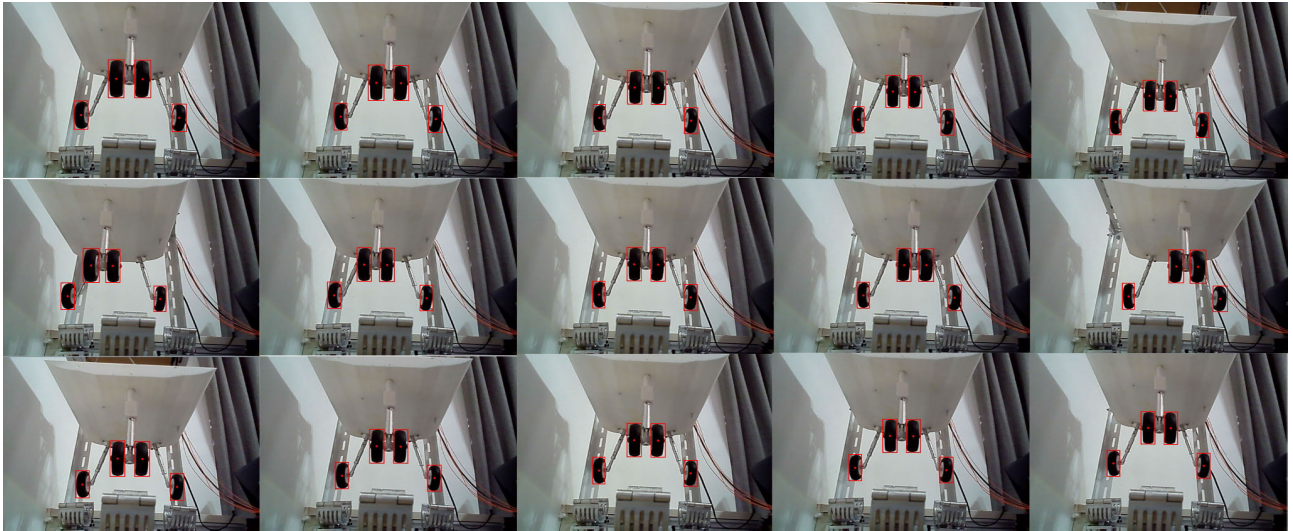
FIGURE 10. Feature recognition with X-direction movement (upper row), Y-direction movement (middle row), Z-direction movement (lower row).
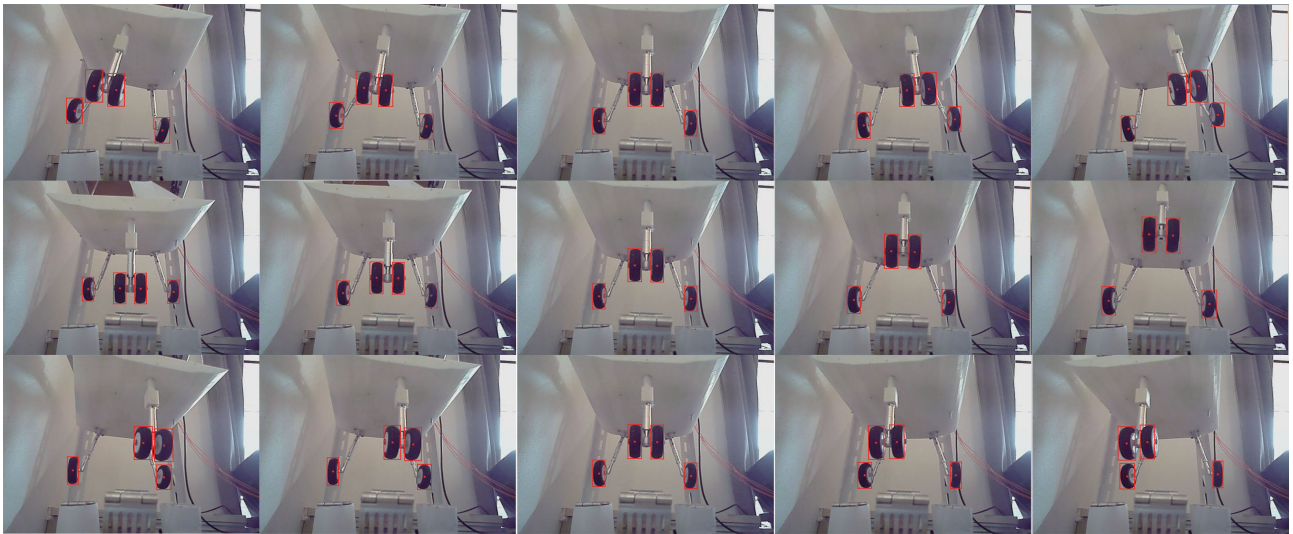

FIGURE 11. Feature recognition with rolling motion (upper row), pitching motion (middle row), yawing motion (lower row).
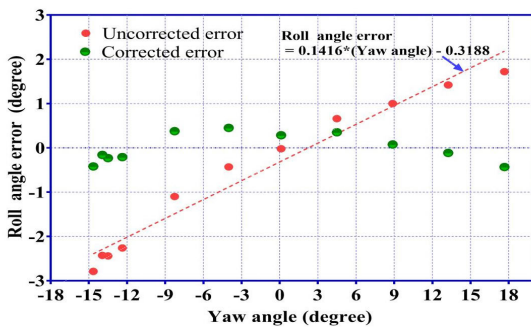

FIGURE 12. Variation of roll angle error with yaw angle in the yawing motion.

noted that, in present experiment, the main factors affecting the accuracy of above solution are the processing error of the lens of the optical system, the pixel resolution, the installation error and the error of measuring the reference value.

IV. Z-DIRECTION CONTROL OF THE CHASER PLATFORM

A. DISCRETE ESTIMATION OF THE Z-DIRECTION POSITION

The process of solving position and attitude would inevitably cause time delay. Therefore, when the chaser platform receives the information about position and attitude of the target landing gear, the latter has already moved and no longer stays at previous state. Thus the chasing trajectory of the chaser platform fails to catch up with the trajectory of the target landing gear, see the "Track 1" in Fig. 16. In order to solve the time delay problem, position prediction for the target landing gear at next time step is made by analyzing the data of current time step. Consequently the chaser platform can correctly catch up with the target landing gear, see
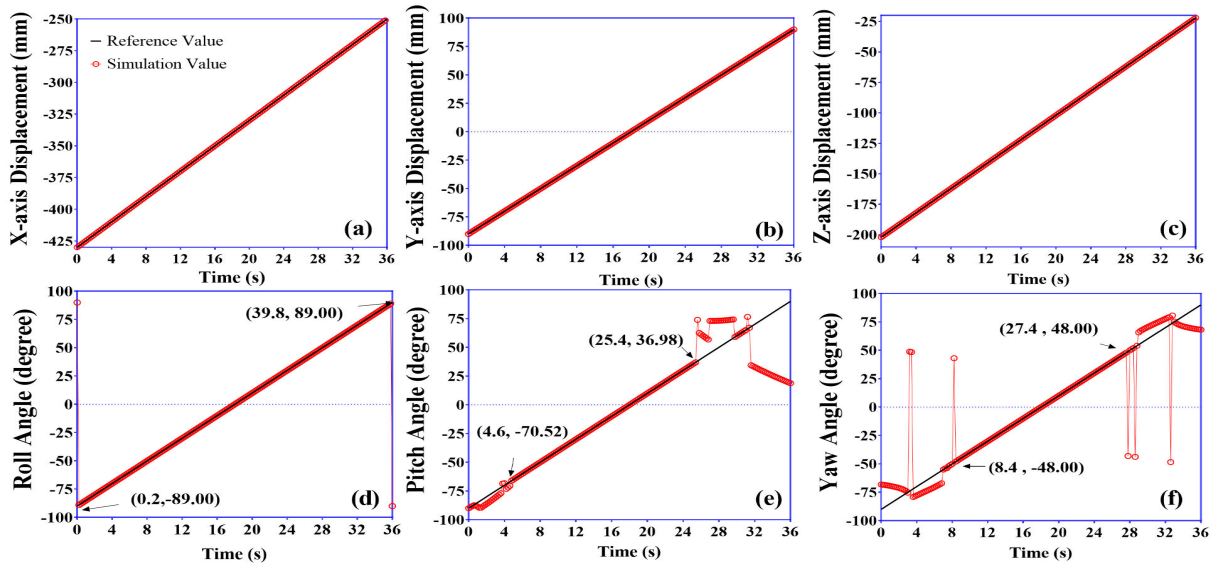
FIGURE 13. Simulated results of the position components and attitude components.
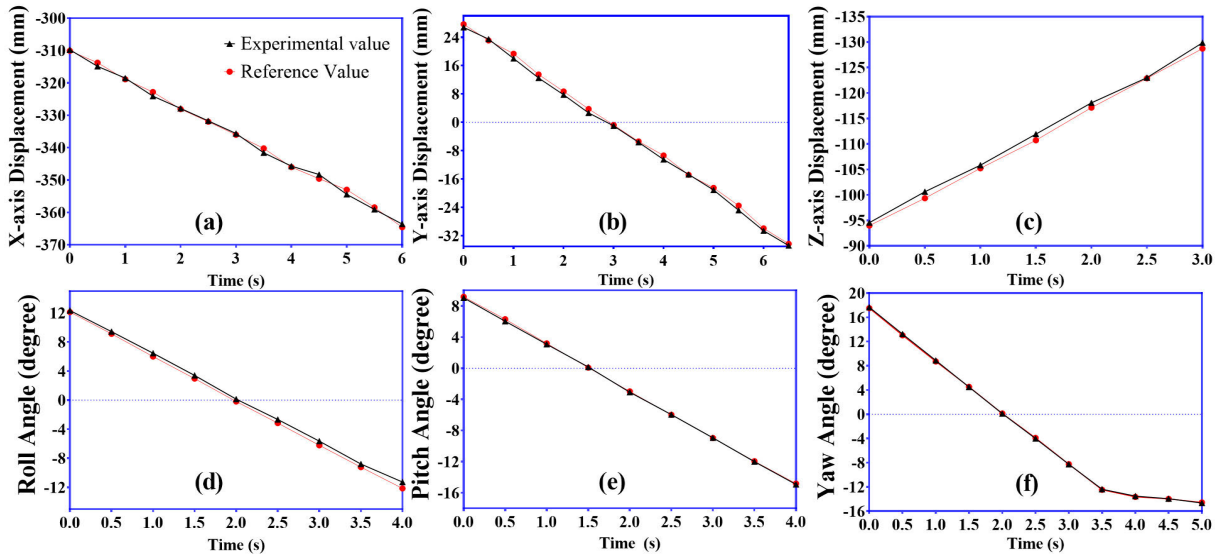
FIGURE 14. Experimental results of the position components and attitude components.

the "Track 2" in Fig. 16. In what follows, the procedure to predict Z-direction position of the target landing gear is given.

The change rate of z-direction displacement is

$$k_{z,i} = \left(z_{t,i} - z_{t,i-1}\right)/T_s, \tag{5}$$

in which i denotes the ith sampling point, $z_{t,i}$ is z-direction coordinate of the target landing gear and T_s is the sampling period. Thus the predicted value of the z-direction coordinate is

$$zp_{t,i+1} = z_{t,i} + k_{z,i} \times \Delta t_i, \tag{6}$$

where Δt_i is time to move to the predicted value (see below) and initially equals to T_s. Then the difference between Z-direction coordinate of the chaser platform $z_{c,i}$ and the predicted Z-direction coordinate of target landing gear $zp_{t,i+1}$ can be computed as

$$S_{z,i} = zp_{t,i+1} - z_{c,i}, \tag{7}$$

and

$$\Delta t_{i+1} = S_{z,i}/v_{z,i}, \tag{8}$$

in which $v_{z,i}$ is Z-direction velocity of the chaser platform. If $\Delta t_{i+1} >= T_s$, then $\Delta t_{i+1} = T_s$ and continue to next
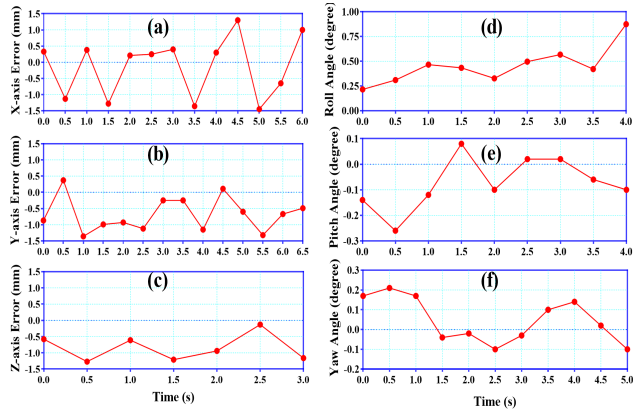
FIGURE 15. Position and attitude errors between experimental value and reference value.
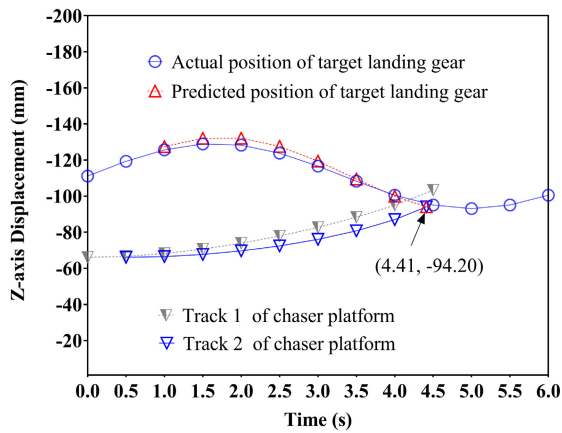

FIGURE 16. Simulation of two different chasing trajectories of the chaser platform. The actual position and predicted position of the target landing gear during the chasing process are also shown.

FIGURE 17. Simulation of chasing trajectory of the chaser platform with different velocities at phase 3. The actual position and predicted position of the target landing gear during the chasing process are also shown.

sampling point. Whereas if $\Delta t_{i+1} < T_s$, the docking operation is going to happen at next time step, and Z-direction coordinate of the target landing gear can be correctly predicted at that moment using (6).

B. Z-DIRECTION SPEED CONTROL OF THE CHASER PLATFORM

During the chasing process from the phase 1 to 3 (as shown in Fig. 8), it is better to keep the chaser platform in a small moving speed [5] and a small constant acceleration. By doing this, it is conducive to reduce the force acting on the chaser aircraft. Therefore the Z-direction speed control strategy for the chaser platform is proposed and tested in this subsection. The speed control is done by imposing a zero initial velocity and velocity at phase 3 (20 mm/s in present experiment. It is shown in Fig. 17 that the value 20 mm/s is appropriate in present case. If the velocity at phase 3 is too slow, such as 5 mm/s, the docking time is predicted to be greater than T_s at the closest point A in Fig. 17, so that the chaser platform will continue to move upwards and cause undesired

collision) and representing z_c, the Z-direction coordinate of the chaser platform in equation (7), by means of quadratic polynomial

$$z_c(t) = C_{z,0} + C_{z,1}t + C_{z,2}t^2, \qquad (9)$$

then v_z (in (8)) can be represented as

$$v_z(t) = C_{z,1} + C_{z,2}t. \qquad (10)$$

A simulation example of the Z-direction speed control is given in the following. In this test, initial velocity of the chaser platform is zero and arrival velocity at phase 3 is 20 mm/s, the sampling period T_s is 0.5 s (this value is determined by considering the GNC loop sampling rate of 0.3 s used in Ref. [5] and the time needed to solve the position and attitude of the target platform) and the target landing gear is imposed to move according to $z_t = -111.2 - 19.0\sin(2\pi ft)$ along the Z-direction, where f is the frequency and equals to 0.15 Hz. Initial Z-direction coordinate of the chaser platform and the target landing gear is $z_{c,0}$ and $z_{t,0}$, respectively. The coefficients $C_{z,0}$, $C_{z,1}$ and $C_{z,2}$ are determined by initial and final Z-direction coordinate and velocity at each time step. The initial position and velocity of next time step are equal to the ones calculated by (9) and (10) at present time step.

The results of this simulation are shown in Fig. 16, in which track 2 of the chaser platform is done by making position prediction of the target landing gear, whereas the track 1 of the chaser platform does not make any prediction. The results shows that both trajectories of the chaser platform satisfy the velocity control equation (10), and the chaser platform keeps small and near constant acceleration during the whole process. It is also seen from Fig. 16 that the successful docking can only be achieved by making position prediction of the target landing gear. Thus the above test proves the soundness of the proposed algorithm for Z-direction control of the chaser platform.
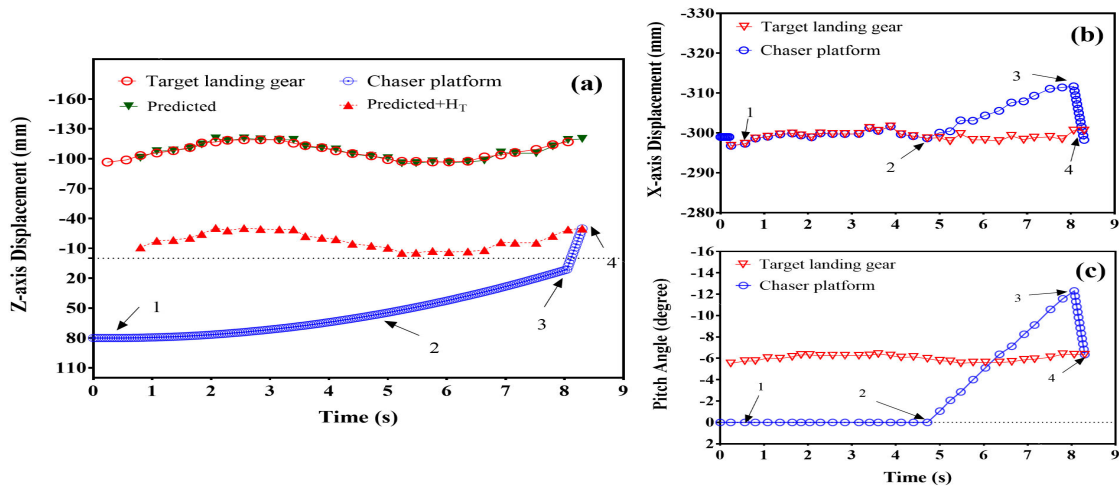
FIGURE 18. Z-direction displacement (panel a), X-direction displacement (panel b) and pitch angle (panel c) of the target landing gear (moving along Z-direction) and the chaser platform.

V. EXPERIMENTAL RESULTS

The experimental results are reported in this Section. The first part describes the docking process when the target landing gear is moving along Z-direction, while the second part describes the docking process when the target landing gear is in compound movement.

A. THE TARGET LANDING GEAR MOVING ALONG Z-DIRECTION

In this test, Console 1 (see Fig. 4) controls the target landing gear to do the Z-direction reciprocating motion. The Z-direction speed of the chaser platform at phase 3 is set to 20 mm/s, position and attitude of the target landing gear are updated every 0.26s, which is determined by the CPU (Core(TM)i7-9750H) performance of Console 2. The experimental results of Z-direction displacement, X-direction displacement and pitch angle of the target landing gear (solved based on monocular vision) and the chaser platform are reported in Fig. 18, in which the curve "Predicted+H_T" means the predicted value of the target landing gear plus the distance H_T (meaning distance between the chaser platform and the target landing gear at phase 4, see Fig. 8).

It is seen from Fig. 18 that the chasing trajectory of the chaser platform can be divided by three main stages. The first stage corresponds to phase 1 to 2 in Fig. 8, where the chaser platform is still far away from the target landing gear and is moving upward slowly with a constant acceleration. The second stage corresponds to phase 2 to 3 in Fig. 8, in order to prevent from blocking the sight of camera during this process, the chasing path planning is made using the theory described in Section III-A2. The third stage corresponds to phase 3 to 4 in Fig. 8, at which the chaser platform blocks the sight of camera and then the position and attitude of the target landing gear cannot be solved. However, the entire time of third stage is quite short (less than T_s), thus the docking
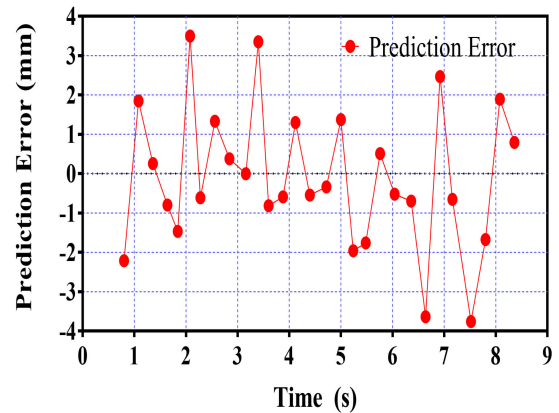

FIGURE 19. The error between predicted and measured Z-direction coordinate value of the target landing gear.

position (at phase 4) is nearly the predicted value obtained at phase 3. It should also be noted that there is no need to perform speed control at third stage due to the short time. The above four phases are all indicated in Fig. 18. Consequently the Z-direction speed of the chaser platform can be effectively controlled by (10) from phase 1 to 3 with constant acceleration. In the meanwhile, the attitude adjustment of the chaser platform during the chasing process can effectively avoid blocking the visual features for attitude algorithm. Furthermore, Fig. 19 reports the error between predicted and measured Z-direction coordinate value of the target landing gear. It is seen that the maximum value will not exceed 4 mm, therefore the design of the docking mechanism should have a redundancy of 4 mm in order to ensure successful docking.

B. THE TARGET LANDING GEAR IN COMPOUND MOVEMENT

When the target landing gear is in a compound movement (meaning that the target landing gear is doing reciprocating
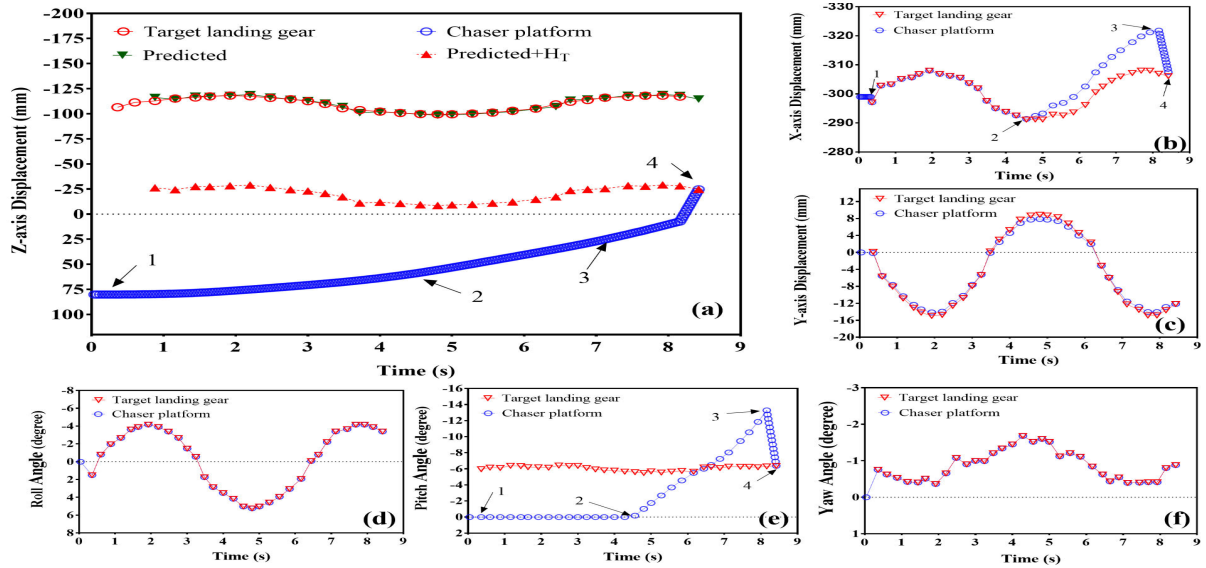
FIGURE 20. Z-direction displacement (a), X-direction displacement (b), Y-direction displacement (c), roll angle (d), pitch angle (e) and yaw angle (f) of the target landing gear (in compound movement) and the chaser platform.
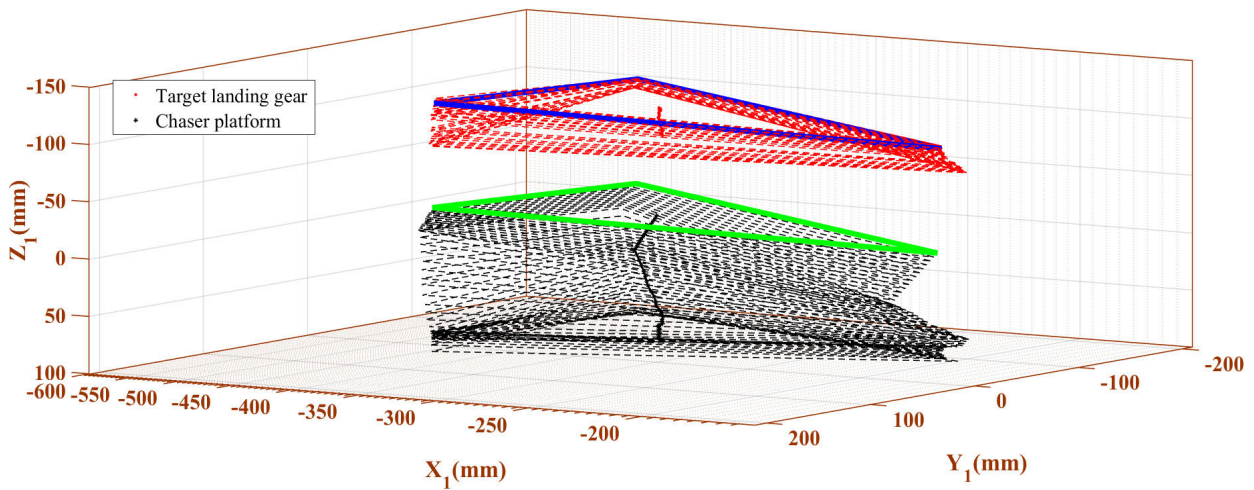

FIGURE 21. Trajectories of the chaser platform (dashed black triangles) and the target landing gear (dashed red triangles).

motion along the X, Y and Z directions, as well as roll, pitch and yaw angles, simultaneously), the chasing trajectory will be much more complex than the one described in last subsection. Fig. 20 reports the variation of six components (X, Y, Z displacements and roll, pitch, yaw angles) of the target landing gear and the chaser platform in present case. The results show that the curve "Predicted+H_T" coincides with the trajectory of the chaser platform at phase 4, indicating that successful docking is also achieved in present complex compound movement. Hence the proposed visual based navigation docking scheme is able to work under the case of complex compound movement. Moreover, in order to have a more clear look at the docking process, Fig. 21 reports

the moving trajectories (in which a triangle corresponds to three points of the target landing gear or the chaser platform) of the target landing gear (dashed red triangles, while blue triangle denotes final position at phase 4) and the chaser platform (dashed black triangles, while green triangle denotes final position at phase 4) in the navigation docking coordinate system. The red solid line is the trajectory of point O_2 in the navigation docking coordinate system, while the black solid line indicates the trajectory of point O_3. Correspondingly, Fig. 22 shows the images collected by the monocular camera during the docking process, the evolution time is indicated in the figure. The variations of position and attitude of both the target landing gear and the chaser platform can thus be
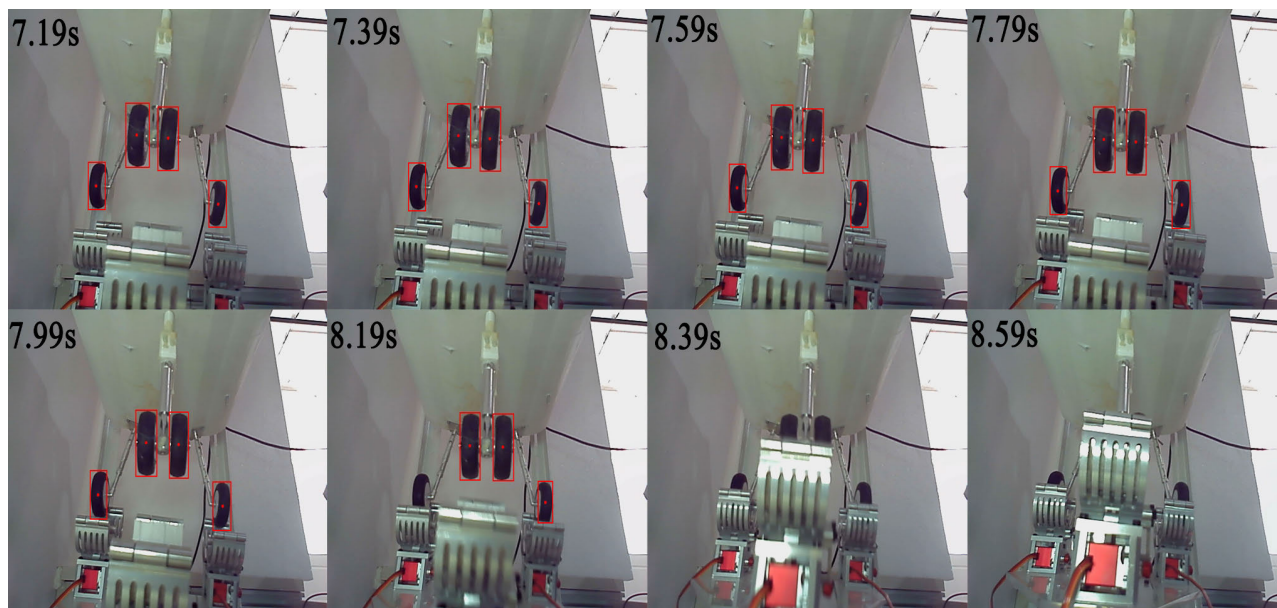
FIGURE 22. Feature recognition during the docking process when the target landing gear is in compound movement, the evolution time is indicated in the panels.

clearly seen from above figures, the chaser platform adjusts its position and attitude in line with the complex compound movement of the target landing gear.

VI. CONCLUSION

A new visual based navigation docking scheme has been proposed and tested numerically and experimentally for the docking of two vertical compound aircraft in flight. An experimental testbed, made of two 6-DOF platforms (the chaser platform and target platform), was built for testing the proposed scheme on the ground. The chaser platform is equipped with a monocular camera to acquire image and then the position and attitude of the target landing gear with respect to the chaser platform are solved based on monocular vision with the theory of solving the P3P problem. In order to prevent the chaser platform from blocking the sight of camera during the chasing process, the attitude of the chaser platform must be adjusted to reduce the blind area of vision acquisition. Therefore a new path and attitude planning algorithm is proposed for the chaser platform. The Z-direction position of the target landing gear is predicted in advance to compensate for the time delay of solving the position and attitude, by doing this the docking accuracy is within 4 mm. Moreover, a Z-direction speed control algorithm is also proposed to control the speed of the chaser platform during the chasing process, thus the acceleration of the chaser platform is small and near constant.

The soundness of the new visual based navigation docking scheme has been proved in following two cases, i.e., the target landing gear is moving along Z-direction and the target landing gear is in compound movement, the experimental results show that both cases result in successful docking. It should be noted that the present scheme can be exploited for many other applications, such as the space rendezvous and docking operations, besides the docking process of vertical compound aircraft.

ACKNOWLEDGMENT

REFERENCES

[1] S. A. McGill, J. A. Schetz, and W. H. Mason, "Compound aircraft transport: A comparison of wingtip-docking and close-formation flight," in *Proc. 41st Aerosp. Sci. Meeting Exhib.*, AIAA Paper, Paper 2003-0607.

[2] A. Behrens, T. Grund, C. Ebert, R. Luckner, and J. Weiss, "Investigation of the aerodynamic interaction between two wings in a parallel flight with close lateral proximity," *CEAS Aeronaut. J.*, vol. 11, no. 2, pp. 553–563, Jun. 2020.

[3] P. Griesemer, J. Mueller, and M. Paluszek, "System design of a reusable, horizontal take-Off/Horizontal landing two stage to orbit vehicle," in *Proc. 46th AIAA/ASME/SAE/ASEE Joint Propuls. Conf. Exhib.*, Jul. 2010, pp. 2010–7169.

[4] G. B. Palmerini, M. Sabatini, A. Pisculli, and P. Gasbarri, "Ground tests of a rendezvous maneuver based on visual servoing," in *Proc. IEEE Aerosp. Conf.*, Mar. 2014, pp. 1–14.

[5] M. Sabatini, G. B. Palmerini, and P. Gasbarri, "A testbed for visual based navigation and control during space rendezvous operations," *Acta Astronautica*, vol. 117, pp. 184–196, Dec. 2015.

[6] D. Ivanov, M. Koptev, M. Ovchinnikov, S. Tkachev, N. Proshunin, and M. Shachkov, "Flexible microsatellite mock-up docking with non-cooperative target on planar air bearing test bed," *Acta Astronautica*, vol. 153, pp. 357–366, Dec. 2018.

[7] C. E. Anderson, "Windtip coupling at 15,000 feet-dangerous experiments," *Flight J.*, vol. 5, no. 6, pp. 64–72, 2000.

[8] M. Mokuno and I. Kawano, "In-orbit demonstration of an optical navigation system for autonomous rendezvous docking," *J. Spacecraft Rockets*, vol. 48, no. 6, pp. 1046–1054, Nov. 2011.

[9] G. Casonato and G. B. Palmerini, "Visual techniques applied to the ATV/1SS rendezvous monitoring," in *Proc. IEEE Aerosp. Conf.*, Mar. 2004, pp. 613–625.

[10] G. Palmerini, M. Sabatini, and P. Gasbarri, "Analysis and tests of visual based techniques for orbital rendezvous operations," in *Proc. IEEE Aerosp. Conf.*, Mar. 2013, pp. 1–14.

[11] Y. Huo, Z. Li, and F. Zhang, "Fast and accurate spacecraft pose estimation from single shot space imagery using box reliability and keypoints existence judgments," *IEEE Access*, vol. 8, pp. 216283–216297, 2020.

[12] J. Ghommam and M. Saad, "Autonomous landing of a quadrotor on a moving platform," *IEEE Trans. Aerosp. Electron. Syst.*, vol. 53, no. 3, pp. 1504–1519, Jun. 2017.

[13] D. Luo, J. Shao, Y. Xu, and J. Zhang, "Docking navigation method for UAV autonomous aerial refueling," *Sci. China Inf. Sci.*, vol. 62, no. 1, pp. 1–16, Jan. 2019.

[14] T. M. Faure, L. Hétru, and O. Montagnier, "Aerodynamic features of a two-airfoil arrangement," *Experim. Fluids*, vol. 58, no. 10, p. 146, Oct. 2017.

[15] P. Ma, Y. Bai, J. Zhu, C. Wang, and C. Peng, "DSOD: DSO in dynamic environments," *IEEE Access*, vol. 7, pp. 178300–178309, 2019, doi: 10.1109/ACCESS.2019.2958374.

[16] X.-S. Gao, X.-R. Hou, J. Tang, and H.-F. Cheng, "Complete solution classification for the perspective-three-point problem," *IEEE Trans. Pattern Anal. Mach. Intell.*, vol. 25, no. 8, pp. 930–943, Aug. 2003, doi: 10.1109/TPAMI.2003.1217599.

[17] F. I. Pereira, J. A. Luft, G. Ilha, and A. Susin, "A novel resection–intersection algorithm with fast triangulation applied to monocular visual odometry," *IEEE Trans. Intell. Transp. Syst.*, vol. 19, no. 11, pp. 3584–3593, Nov. 2018, doi: 10.1109/TITS.2018.2853579.

[18] X. Zhuo, "A note on unique solution conditions of the P3P problem," *Chin. J. Comput.*, vol. 26, no. 12, pp. 1696–1701, 2003.

[19] D. DeMenthon and L. S. Davis, "Exact and approximate solutions of the perspective-three-point problem," *IEEE Trans. Pattern Anal. Mach. Intell.*, vol. 14, no. 11, pp. 1100–1105, Nov. 1992.

[20] A. Dumlu and K. Erenturk, "Modeling and trajectory tracking control of 6-DOF RSS type parallel manipulator," *Robotica*, vol. 32, p. 643, Jul. 2014.

DONG WANG received the B.E. degree from Hebei Union University, Tangshan, China, in 2014. He is currently pursuing the Ph.D. degree with the Changchun Institute of Optics, Fine Mechanics and Physics, Chinese Academy of Sciences, China. His main research interest includes design of compound aircraft.

QIZHEN HONG received the B.E. degree from the Beijing University of Aeronautics and Astronautics, in 2017. He is currently pursuing the Ph.D. degree with the Institute of Mechanics, Chinese Academy of Sciences. His research interests include high-fidelity modeling of high temperature flows, quantum-classical calculation for rate coefficients, and the design of compound aircraft.

JING WANG is currently a Research Fellow and a Supervisor of the Ph.D. candidates with the Changchun Institute of Optics, Fine Mechanics and Physics, Chinese Academy of Sciences, China. Her main research interests include optical precision instrument design and photoelectric imaging technology research.

HERAN SUN received the B.E. degree from the Changchun University of Technology and Science, Changchun, China, in 2013. He is currently pursuing the Ph.D. degree with the Changchun Institute of Optics, Fine Mechanics and Physics, Chinese Academy of Sciences, China. His main research interest includes optical meta-materials.

LUCHAO CHENG received the B.E. and M.S. degrees from Jilin University, Changchun, China, in 2012 and 2015, respectively. He is currently pursuing the Ph.D. degree with the Changchun Institute of Optics, Fine Mechanics and Physics, Chinese Academy of Sciences, China. His main research interest includes composite structures design.
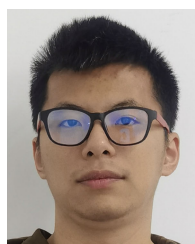

MINGYANG LI received the B.E. degree from Yangtze University, Jingzhou, China, in 2018. He is currently pursuing the Ph.D. degree with the Changchun Institute of Optics, Fine Mechanics and Physics, Chinese Academy of Sciences, China. His main research interest includes detection and tracking of drone swarm targets.

CONGJING WANG was born in An Hui. She received the B.E. degree from the Harbin Institute of Technology, Weihai, China, in 2018. She is currently pursuing the M.S. degree with the Changchun Institute of Optics, Fine Mechanics and Physics, Chinese Academy of Sciences, China. Her main research interest includes structure design of photoelectric measurement and control equipment.

XIN HUANG received the B.E. degree from Southwest Jiaotong University, Chengdu, China, in 2017. He is currently pursuing the M.S. degree with the Changchun Institute of Optics, Fine Mechanics and Physics, Chinese Academy of Sciences, China. His main research interests include photoelectric imaging and measurement technique.

ZHIYUAN WANG received the B.E. degree from Northeastern University, Qinhuangdao, China, in 2018. He is currently pursuing the Ph.D. degree with the Changchun Institute of Optics, Fine Mechanics and Physics, Chinese Academy of Sciences, China. His main research interest includes image processing.

JIAHANG LI is currently pursuing the B.E., MA.Eng., and Ph.D. degrees with the Beijing Institute of Technology, Beijing, China. She is studying in the genius class of Teli College.

• • •